NASA Contractor Report 198428

Structural Evaluation of a Space Shuttle Main Engine (SSME) High Pressure Fuel Turbopump Turbine Blade

Ali Abdul-Aziz
NYMA, Inc.
Brook Park, Ohio

June 1996

Prepared for
Lewis Research Center
Under Contract NAS3–27186

National Aeronautics and
Space Administration

STRUCTURAL EVALUATION OF A SPACE SHUTTLE MAIN ENGINE (SSME) HIGH PRESSURE FUEL TURBOPUMP TURBINE BLADE

Ali Abdul-Aziz
NYMA, Inc.
2001 Aerospace Parkway
Brook Park, Ohio 44142

SUMMARY

Thermal and structural finite-element analyses were performed on the first high-pressure fuel turbopump turbine blade of the space shuttle main engine (SSME). A two-dimensional (2-D) finite-element model of the blade and firtree disk attachment was analyzed using the general purpose MARC (finite-element) code. The loading history applied is a typical test stand engine cycle mission, which consists of a startup condition with two thermal spikes, a steady state, and a shutdown transient. The blade material is a directionally solidified (DS) Mar-M 246 alloy, the blade rotor is forged with waspalloy material. Thermal responses under steady-state and transient conditions were calculated. The stresses and strains under the influence of mechanical and thermal loadings were also determined. The critical regions that exhibited high stresses and severe localized plastic deformation were the blade-rotor gaps.

INTRODUCTION

The purpose of this study is to better understand the blade damage modes and failure characteristics caused by the high mechanical loads and the severe thermal transients exhibited by the space shuttle main engine (SSME). Typically, hot section components of advanced space vehicle engines such as the SSME are exposed to extreme gas pressure and thermal excursions. These operating conditions subject the turbomachinery components to severe thermomechanical cycles that induce high inelastic strain variations and eventual fatigue crack growth.

Thus, the goal of this work is to analyze the blade under these severe operating conditions and to determine the stress-strain fields in the SSME blade to enable life prediction studies. The MARC (ref. 1) finite-element code is used for the analysis.

FINITE-ELEMENT MODELING

The blade finite-element model is shown in figure 1. The mesh consists of 3549 plane strain elements and 4000 nodes. The blade firtree attachments were modeled with 70 bilinear connecting gap elements. This model was obtained from Marshal Space Flight Center (MSFC) (ref. 2). The actual blade is illustrated in figure 2. It has a length of 4.19 cm with an airfoil span length of 2.2 cm and a span-to-chord-width aspect ratio of approximately unity. The blade is made of a cast nickel-base alloy MAR-M 246 (+hf) DS material. It is directionally solidified by a casting method that produces long grain boundaries along the axial direction and minimizes those along the transverse direction. With the directional solidification technique, the properties developed in the direction of solidification (longitudinal direction) differ from those in the orthogonal direction. A careful consideration was given to implementing these directionality effects, including temperature dependency, in the analyses.

The blade rotor is forged with waspalloy material that is a vacuum-melted, precipitation-hardened, nickel-base alloy, which is strengthened by the precipitation of titanium and aluminum components and the solid-solution strengthening effects of chromium, molybdenum, and cobalt. The material properties for all the alloys used in these analyses were obtained from Rockwell International Corporation (personal communication, Rockwell International Corporation, Rocketdyne Division, 1992). Tables I to IV list the values of the physical and mechanical properties of these alloys.

ANALYTICAL PROCEDURE

The analytical portion of this study was initiated by conducting a heat transfer analysis followed by a subsequent stress analysis. The mission cycle used consisted of the turbine inlet temperature, the gas pressure, and the rotational speed. Figures 3(a) to (d) represent the variation of these parameters as a function of elapsed time. This cycle is applicable to a factory test of the engine, and it closely represents a flight mission except for the steady-state operating time which was cut to only 24 sec. Thermal transients caused by the ignition spikes during the startup and shutdown conditions are thought to be the major factor inducing high thermal stresses. These high stresses can cause fatigue failure and eventually lead to cracking.

HEAT TRANSFER

The geometric complexity of the SSME blade made the imposition of the thermal boundary conditions quite cumbersome. Several assumptions were made. However, the primary emphasis was directed at obtaining temperature distribution and gradients for the blade-firtree interface. The goal was to obtain the best estimates of the boundary conditions at various convective heat transfer zones.

The following assumptions were considered in the analysis. (1) Areas of contact at the firtree lobes were equal on either side of the blade. (2) The thermal contact resistance between the firtree and the disk attachment was assumed to be zero, because empirical relations for the thermal contact resistance under high pressures (approximately 689 MPa) are practically unavailable and contact resistance decreases rapidly with increasing pressure. (3) The gas temperature was assumed to be constant with each time step. (4) The thermal effect of the coating material typically used on the airfoil and on the shank was not accounted for.

Also, it must be pointed out that at the high rotational speed of approximately 38 000 rpm, the values of applicable convective heat transfer correlations are approximated since this speed exceeds the range of the currently available correlations and data. Heat transfer coefficients over the airfoil were obtained from reference 3. Additional details regarding the computations and the magnitude of the film coefficients for both pressure and suction sides are also available in reference 3.

A correlation for the heat transfer coefficient for a circular cylinder in a cross flow was used as a means for predicting the film coefficients at the leading-edge zone (ref. 4). This correlation included turbulent flow effects. The trailing edge and the blade tip areas were assigned heat transfer coefficients averaged from the adjacent values of the pressure and suction sides.

For the shank region, heat transfer correlations for a uniform temperature surface over a flat plate were used (ref. 5). The length parameter in the Reynolds number was taken as the surface length at the shank mid-span, measured from an approximate location of the leading-edge stagnation region. A Reynolds number of 500 000 was used as a criteria for transition. The cross-sectional area formed by the flow passage between two blade shanks was used to calculate an average flow velocity, from which appropriate Reynolds numbers were obtained. Figure 4 shows the calculated film coefficients used for the shank region. The assumed correlations used in these calculations, as obtained from reference 5, are:

$$\mathrm{Nu} = 0.0288\,\mathrm{Re}^{0.8}\,\mathrm{Pr}^{1/3}, \mathrm{Re} > 5\times10^{5} \tag{3}$$

$$\mathrm{Nu} = 0.332\,\mathrm{Re}^{0.5}\,\mathrm{Pr}^{1/3}, \mathrm{Re} \le 5\times10^{5} \tag{4}$$

Where Re is the Reynolds number based on the average flow velocity and the surface length on the pressure and suction side, and Pr is the prandlt number of the working fluid.

For the platform region, free-stream velocities next to the top of the platform were assumed to be equal to the respective velocities around the airfoil, and adjacent airfoil heat transfer coefficients were used for the convective elements of the platform edges. Estimation of the average heat transfer coefficients in the gaps was done by using the correlation of Morris and Woods for flow in pipe rotating about a parallel axis, which is given in reference 6. The following equation illustrates this correlation.

$$\mathrm{Nu} = 0.0102\,\mathrm{Re}_{dh}^{0.78}\,\mathrm{Re}_{\Omega}^{0.25}\,\mathrm{Pr}^{0.4} \tag{5}$$

Where Re_{dh} is the Reynolds number based on the pipe hydraulic diameter, Re_{Ω} is the rotational Reynolds number.

Boundary conditions such as the cooling effects by the hydrogen fuel of the blade from the disk attachment region were imposed via the MARC code user's subroutine (ref. 1). Similarly, the film coefficients, hot gas temperature, and Reynolds number histories at full power level conditions were also added in the thermal model. Transient boundary conditions for both heated and cooled surfaces along the airfoil were obtained by scaling the values of the boundary conditions according to the transient flow and temperature. In this procedure, the steady-state heat transfer coefficients were adjusted by a factor equal to the ratio of the Reynolds number at any period over the steady-state Reynolds number. This ratio was raised to the power of 0.8, a value assumed based on the correlations for heat transfer coefficients over a flat plate, indicating that the heat transfer rate is proportional to the power of 0.8 for a turbulent flow. This procedure has been found to be appropriate and yields satisfactory results (ref. 4)

STRUCTURAL ANALYSIS

Two-dimensional, structural, finite-element analyses of the SSME high-pressure turbine blade were carried out under the influence of centrifugal, gas pressure, and thermal loadings. The mission history represented in figure 3 was used for both the thermal and the structural analyses. The analyses employed full power level conditions, which include the first and second ignition spike temperatures during the startup period of the engine. Also, cruise and shutdown conditions for gas temperature, gas pressure, and rotational speed were employed.

The friction gap elements used to model the contact between the firtree and the rotor proved to be computationally nonefficient. Therefore, to override this obstacle, the tying constraint option available within the MARC code was employed to simulate the contact between the firtree and rotor disk. This was invoked by duplicating the nodes along the contact region and tying only the contacting nodes.

The mechanical and thermal properties for the materials, (waspalloy and MAR-M 246), were supplied to the code by defining a yield criterion and a strain hardening law. Other factors of all the physical properties employed, such as temperature dependency, were included in the analysis as well. Tables I to V show the properties of the materials and the stress-strain data from references 2 and 3, which were used as a function of temperature for both alloys. Elastic-plastic calculations were based on the incremental plasticity theory that uses the von-Mises-yield criterion, the normality rule, and a kinematic hardening model. The elastic-plastic behavior of the material was specified by yield strengths and work-hardening properties in the longitudinal and transverse directions. Residual load corrections were applied to ensure that equilibrium was maintained at the start of each new increment.

The blade was constrained so that the edges of the rotor were free to move in the radial direction and fixed along the hoop direction. This was accomplished by transforming the nodes along the snaps of the blade and rotor lobes into a local cylindrical system, in which the nodes were fixed along the normal direction to the contact surface and were allowed to slide with respect to each other in the horizontal direction.

RESULTS AND DISCUSSIONS

The results obtained from the finite-element analysis are shown in figures 5 to 15. These figures show the metal temperature and the von-Mises-equivalent stresses of the blade under transient conditions. The critical region of interest was along the blade and rotor snaps, as expected. However, the location of the highest strain range is near the fourth lobe at both disk-rotor and blade at the right side.

The calculated metal temperature at the critical region is shown in figure 5 as a function of elapsed time. The temperature at the first and second ignition spike conditions are shown in figures 6 and 7. A uniform temperature distribution at the airfoil is clearly visible for both cases, however this trend changes as it reaches the platform, firtree, and disk attachments. This is due to the effects of the difference in the thermal environment caused by the mixture of the cold and hot gases. Also, the temperature reaches a maximum of about 1135 °C during the first spike at the airfoil section (fig. 6). At the firtree-rotor region the temperature remained nearly symmetric along both pressure and suction sides which is a clear indication of the symmetric thermal boundary conditions imposed. However, the thermal gradient, as a result of the cold-hot gases mixture through the lobe gaps, is quite obvious at all locations (figs. 6 to 8). This phenomena is due to the complex configuration of the rotor and the relative magnitudes of the coolant gas flow rates involved. The nonuniformity of the forward and aft seal clearances of the platform may be an additional explanation, which suggests that circumferential and radial variations of gas temperature can exist at the firtree and shank forward face areas.

The second-ignition-spike temperature distributions are shown in figure 7. A sharp increase in the temperature level towards the center of the airfoil is noted, which illustrates the effects of the oscillations caused by the fuel flow rates at this particular time.

The steady-state or cruise condition of the blade temperature is represented in figure 8. The blade airfoil temperature is uniform and the temperature decreases to a lower magnitude near firtree-rotor attachments. The maximum temperature is about 790 °C at the airfoil and the minimum is around –37 °C near the base of the firtree and disk rotor. Figure 9 shows the temperature at the engine shutdown condition.

Figures 10 and 11 show the temperature gradient along the span and cord directions, respectively. These two figures represent the severity of the thermal gradient in the key regions of the blade such as the shank and the platform. However, the accuracy of the heat transfer coefficients and the fluid temperatures at these areas can have significant impact on the thermal gradient.

The von-Mises-equivalent stresses for the blade are shown in figures 12 to 15. Figure 12 shows the stress distributions during the first ignition spike. For instance, at this time, the stresses are thermally driven only. The magnitude of the stresses reaches 862 MPa and the distribution is nonuniform, especially at the firtree-disk rotor interface region. This sharp increase in the stress is due to the high temperature experienced by the blade because of the sudden increase in hot gas pressure during ignition startup.

At the second spike condition, the stresses are slightly higher than those of the first spike. This is due to the combined effects of both thermal and mechanical loads. However, the contributions of the thermal loads are much higher than those of the mechanical load since maximum mechanical loading effects are achieved at cruise conditions when the rotational speed reaches nearly 38 000 rpm.

The stresses under cruise conditions are shown in figure 13. They reflect the effects of all the engine parameters such as speed, pressure, coolant flow, temperature, and thrust. As expected, the maximum stress locations were at the lobes-disk-rotor interface, and their magnitude reached a maximum of 1220 MPa. Figure 14 shows the equivalent stresses under centrifugal loading alone, with a maximum stress level around 1069 MPa. This is 20 percent less than what was recorded at cruise condition when the blade was subjected to combined loading. Clearly, this is an indication of the severe effects caused by the thermal load. However, regions with high stress concentration still remained at the firtree-disk rotor lobes under both loading conditions.

Table VI shows the plastic strains at the critical locations under different intervals during the mission cycle. It is noted that the plastic strain at the critical location increased by about 55 percent when the blade was subjected to combined thermomechanical loading compared to mechanical loading alone. Similar changes occurred at the disk portion also.

Figure 15 represents the stresses during the shutdown period. A sharp drop in the stress level is noted, (a maximum stress of 407 MPa). The existence of high stresses is only seen at the firtree-disk-rotor base interface region where a near cryogenic thermal condition exists.

CONCLUSIONS

A two-dimensional, thermal-structural, finite-element analysis has been conducted on the high pressure fuel turbopump first stage blade of the space shuttle main engine (SSME) under transient and steady-state conditions. A typical engine stand mission cycle was used for the analysis which included temperature, gas pressure, and rotational speed. The following conclusions can be drawn:

(1) Thermal finite-element analysis showed that the blade experienced a high temperature during the first ignition spike (1135 °C). The airfoil temperature remained nearly uniform and independent of what is below the platform region.

(2) The thermal load was shown to influence the stress level in the blade by 20 percent.

(3) The highest stress regions of the blade were found to be at the rotor-firtree lobes with the fourth lobe as the most critical region. Also the blade showed higher plastic strains than the disc rotor throughout the entire mission cycle.

(4) The results obtained in these analyses offer potential benefits to the space shuttle main engine durability studies since they provide a range of thermal and stress-strain data experienced by the blade during engine operation, which would yield a better estimate for the fatigue life of the blade.

REFERENCES

1. MARC General Purpose Finite Element Analysis Program. Vol. A: User Information Manual; vol B: MARC Element Library; MARC Analysis Research Corporation, Palo Alto, California, 1988.
2. Lee, H.: Space Shuttle Main Engine High Pressure Fuel Turbopump Turbine Blade Cracking. NASA TM–100327, 1988.
3. Abdul-Aziz, A. et al: Thermal Finite-Element Analysis of Space Shuttle Main Engine Turbine Blade. NASA TM–100117, 1987.
4. Churchill, S.W.; and Bernstein, M.: A Correlating Equation for Forced Convection From Gases and Liquids to a Circular Cylinder in Crossflow. J. Heat Tran. vol. 99, no. 2, May 1977, pp. 300–306.
5. Kays, W.M.; and Crawford, M.E.: Convective Heat and Mass Transfer. Second ed., Mcgraw-Hill, New York, 1980, pp. 288–312.
6. Stephenson. P.L.: An Experimental Study of Flow and Heat Transfer in a Duct Rotating About a Parallel Axis. Heat and Mass Transfer in Rotating Machinery, pp. 39–49, Hemisphere Publishing Corporation, Washington, DC, 1984.

TABLE I.—PHYSICAL PROPERTIES OF MAR-M 246 DS

Temperature, °C	Thermal coefficient of expansion, α (1/°C)	Thermal conductivity, K (W/(m·K))	Specific heat, Cp (J/(kg·K))
-129	11.3E-5	12.7	399
21	11.3E-5	12.7	399
93	11.3E-5	13.0	399
427	13.0E-5	16.8	420
538	14.1E-5	18.9	441
649	14.9E-5	21.0	462
760	15.6E-5	23.0	483
982	16.8E-4	27.2	525
1093	18.6E-4	30.0	567

TABLE II.—MECHANICAL PROPERTIES OF MAR-M 246 DS

Temperature, °C	E_x, E_y (GPa)	E_z (GPa)	G_{xy} (GPa)	G_{yz}, G_{xz} (GPa)	ν
21	205.47	129.00	71.00	60.65	0.285
93	195.13	126.90	69.70	59.85	0.285
222	196.50	125.50	68.30	58.47	0.287
427	184.80	118.60	63.91	54.88	0.294
538	177.90	115.15	62.12	53.57	0.299
649	167.55	111.70	59.00	50.47	0.312
760	163.41	106.90	57.85	49.44	0.317
871	155.83	102.73	50.95	43.31	0.333
982	151.00	95.10	49.10	42.47	0.341
1093	145.50	93.10	48.00	42.00	0.347

TABLE III.—PHYSICAL PROPERTIES OF WASPALLOY

Temperature, °C	Thermal coefficient of expansion, α (1/°C)	Thermal conductivity, K (W/(m·K))	Specific heat, Cp (J/(kg·K))
21	12.20E-5	10.70	399
93	12.20E-5	11.60	399
222	12.80E-5	12.80	395
427	13.70E-5	16.30	440
538	14.00E-5	18.10	420
649	14.40E-5	20.00	460
760	15.30E-5	21.90	480
870	16.00E-5	24.10	500

TABLE IV.—MECHANICAL PROPERTIES OF WASPALLOY
[G = 80 Gpa; ν = 0.305]

Temperature, °C	E, GPa
21	213.00
93	210.00
222	203.00
427	191.00
538	186.00
649	176.00
760	167.00
870	158.00
982	145.00

TABLE V.—NONLINEAR STRESS-STRAIN CURVE

MAR-M 246 DS		WASPALLOY	
Stress, MPa	Strain, percent	Stress, MPa	Strain, percent
862	0.000	793	0.0000
896	0.200	807	0.2000
931	0.427	820	0.4106
1076	0.597	944	0.5106
1151	0.698	1027	0.7106
1186	0.828	1062	1.5106
1296	3.897	1145	3.9106

TABLE VI.—TOTAL EQUIVALENT PLASTIC STRAIN

Critical location	First spike,[a] percent	Cruise,[a] percent	Cruise,[b] percent
Blade	0.1612	0.8590	0.3844
Disk	0.3259	0.6567	0.03825

[a]Combined thermal-mechanical loading.
[b]Mechanical loading only.

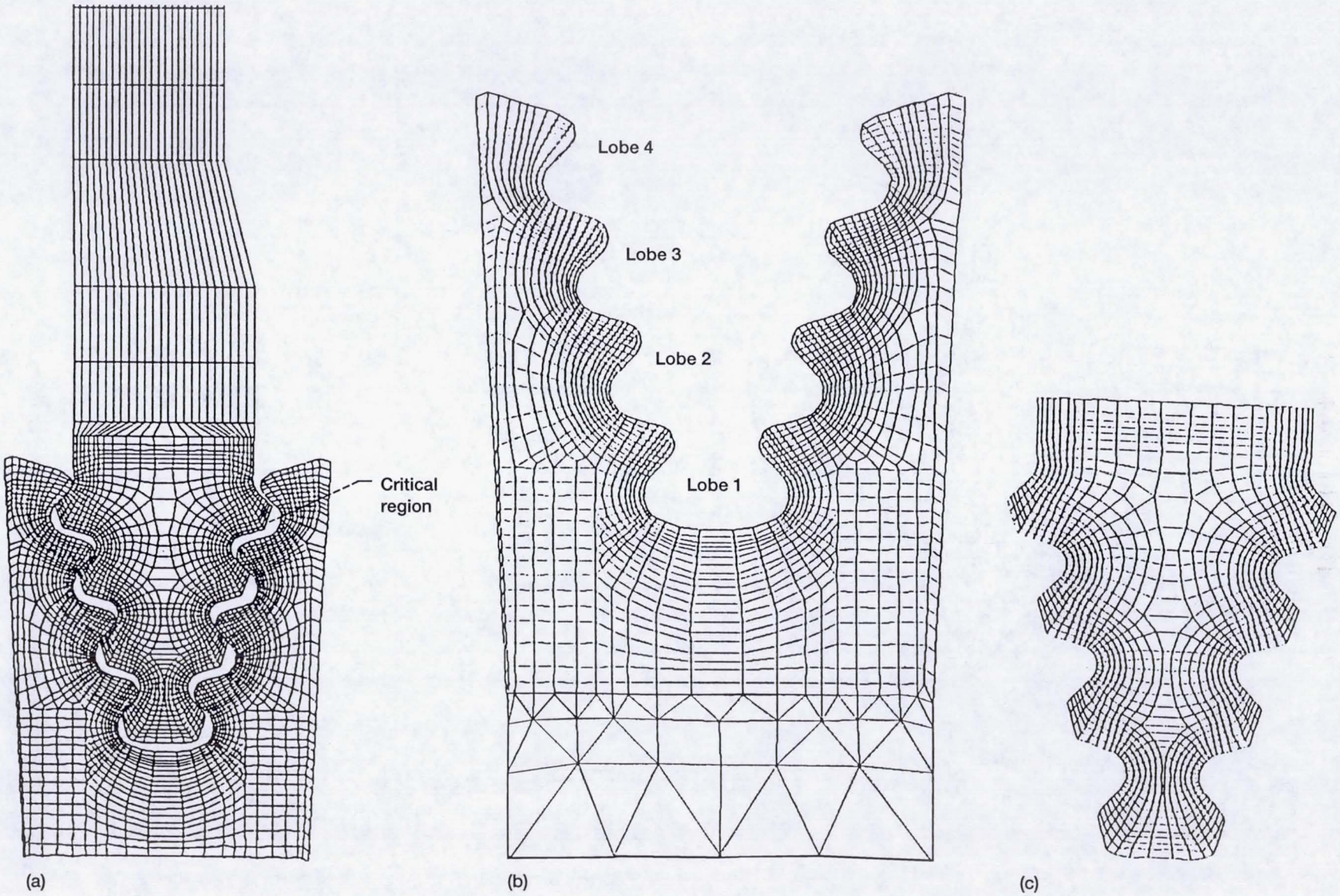

Figure 1.—Finite-element model. (a) Entire blade. (b) Disk-rotor. (c) Firtree.

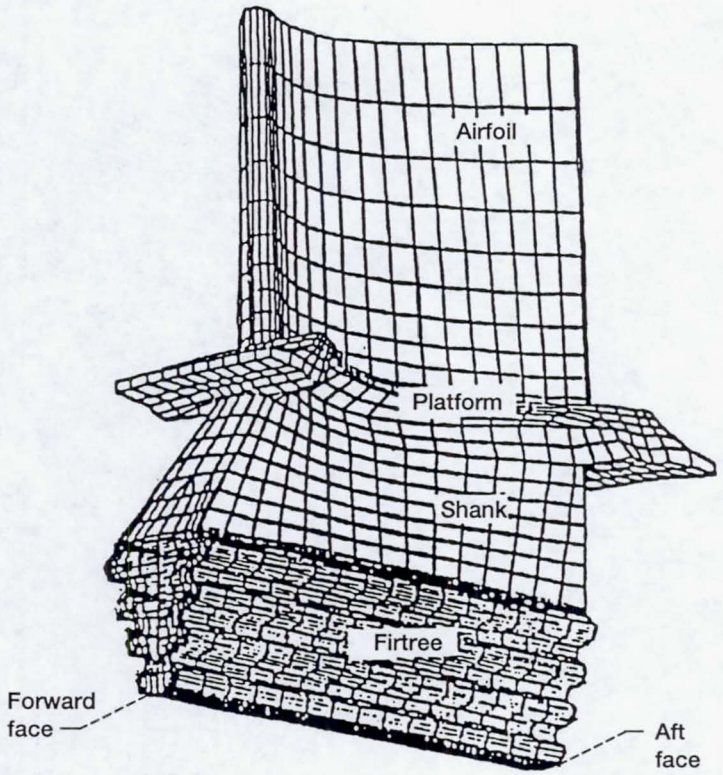

Figure 2.—First stage of SSME blade.

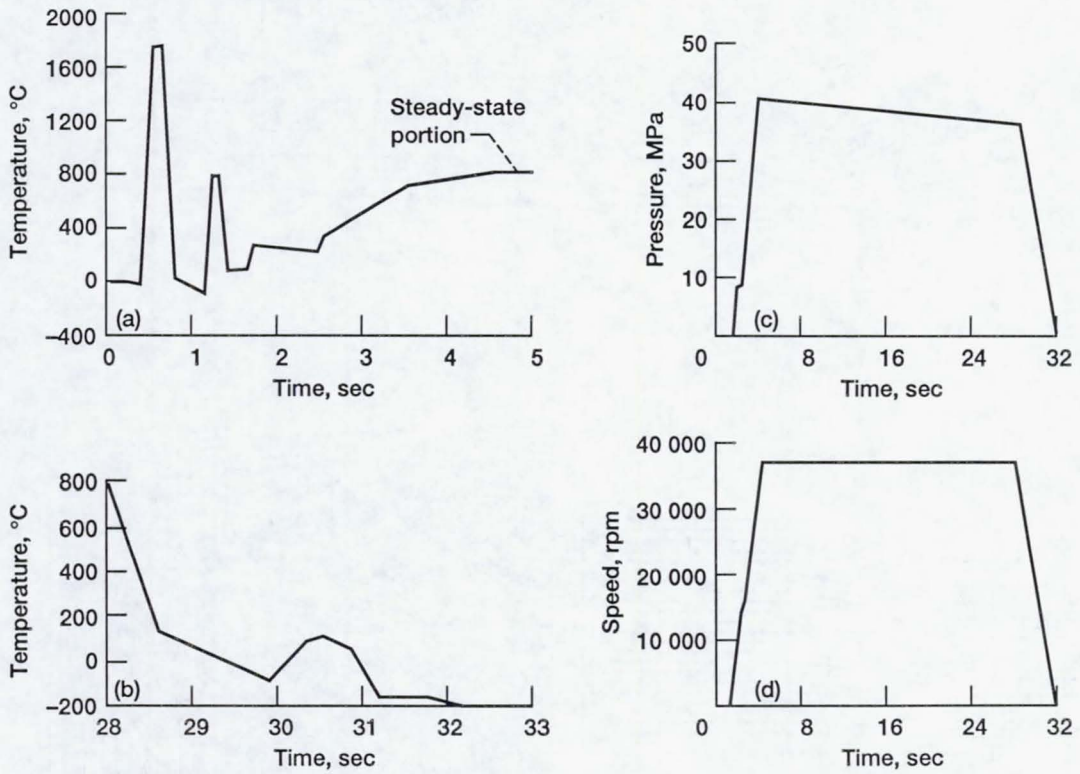

Figure 3.—Mission cycle used for analysis. (a) Start up transient. (b) Cutoff transient. (c) Turbine inlet pressure. (d) Blade rotational speed.

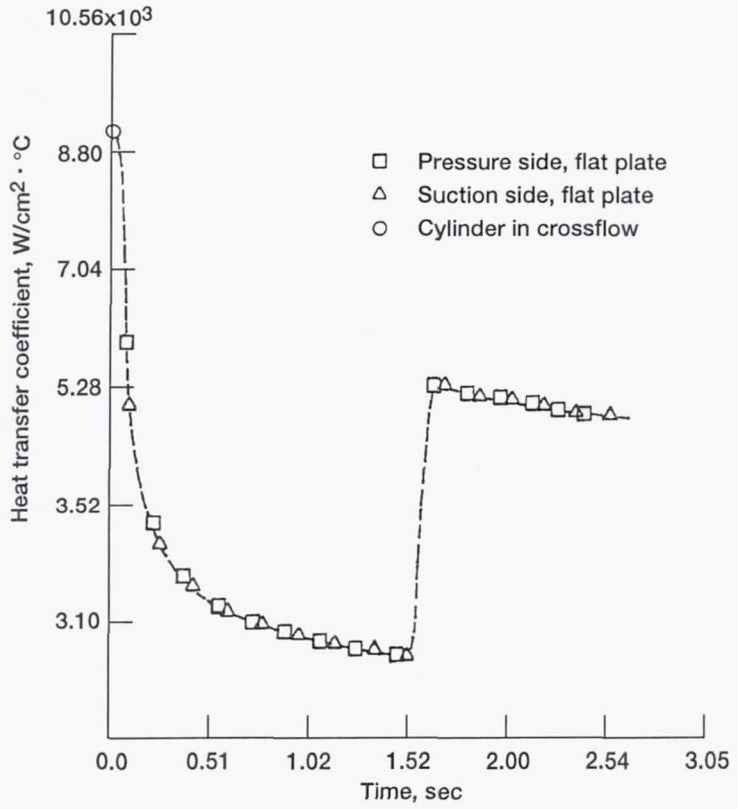

Figure 4.—Heat transfer coefficient at the shank.

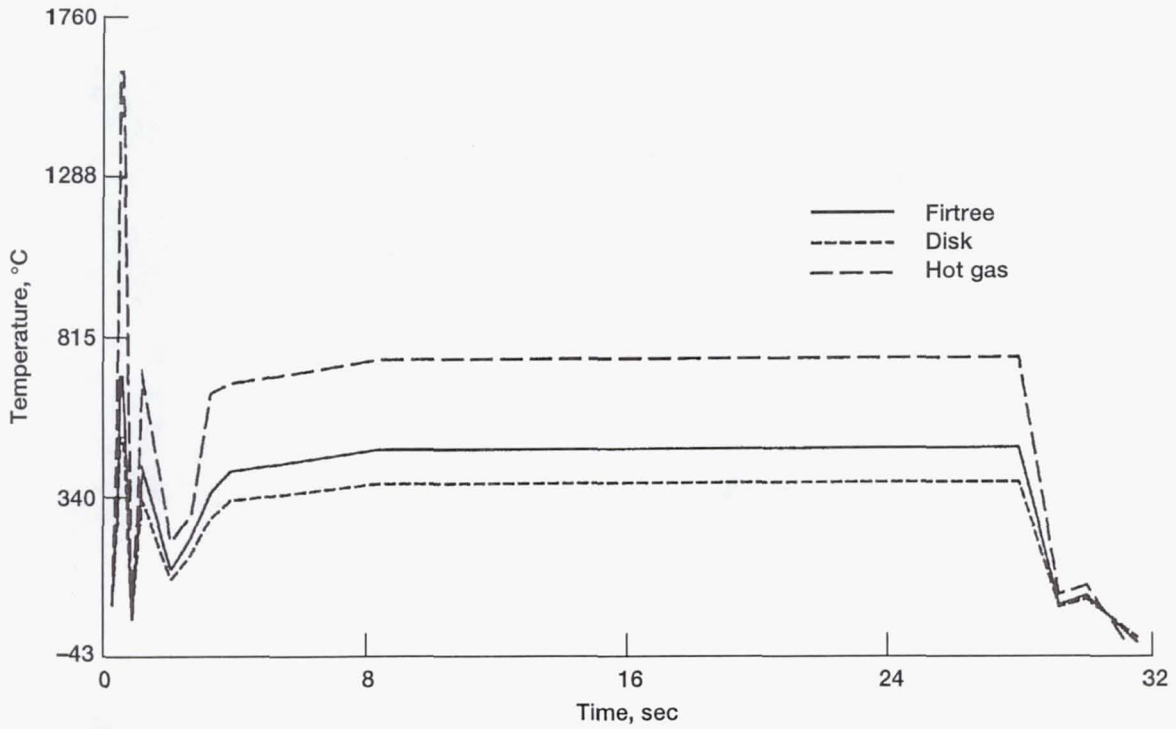

Figure 5.—Calculated metal temperature at critical regions (see fig. 1).

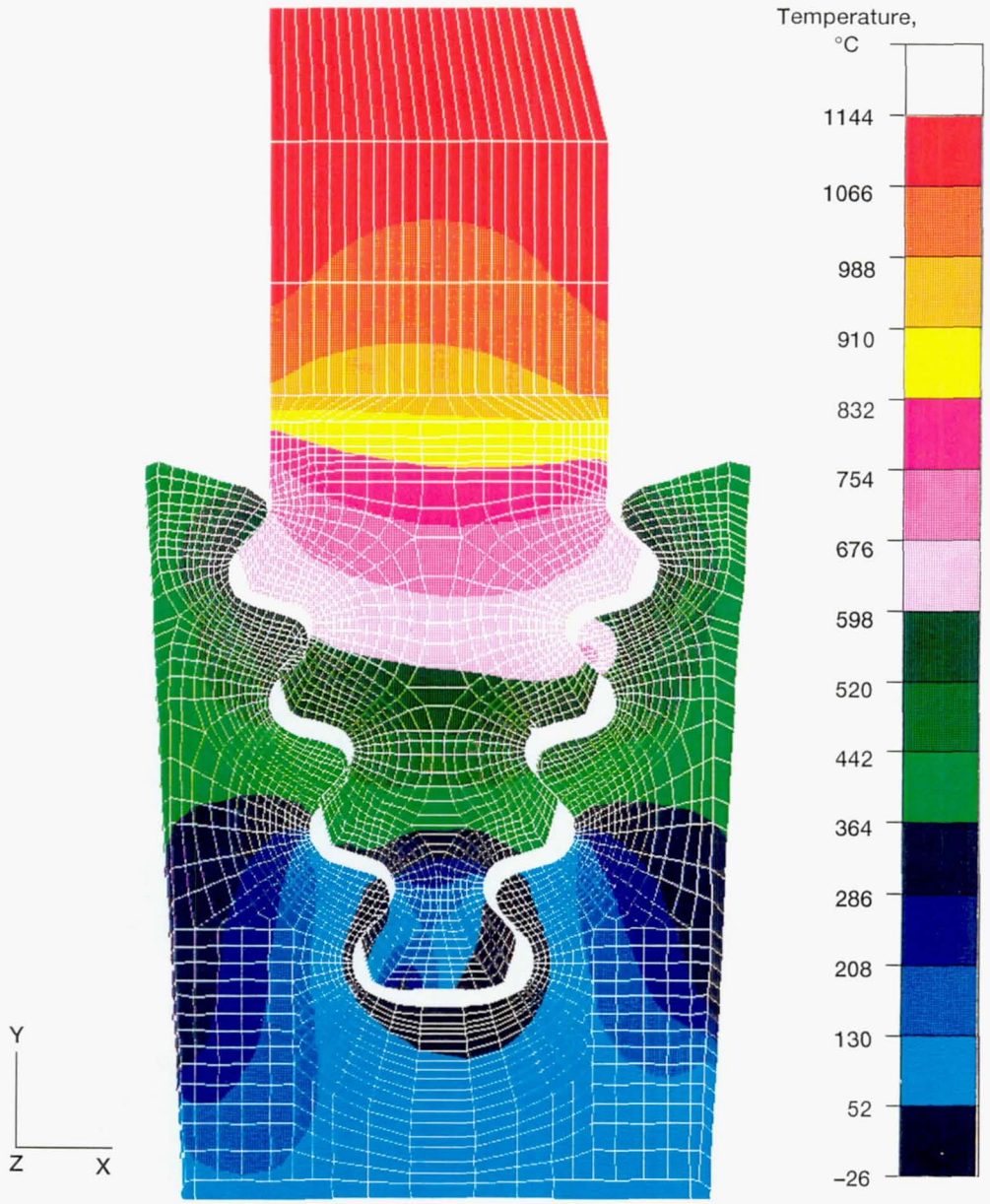

Figure 6.—Temperature at first ignition spike condition.

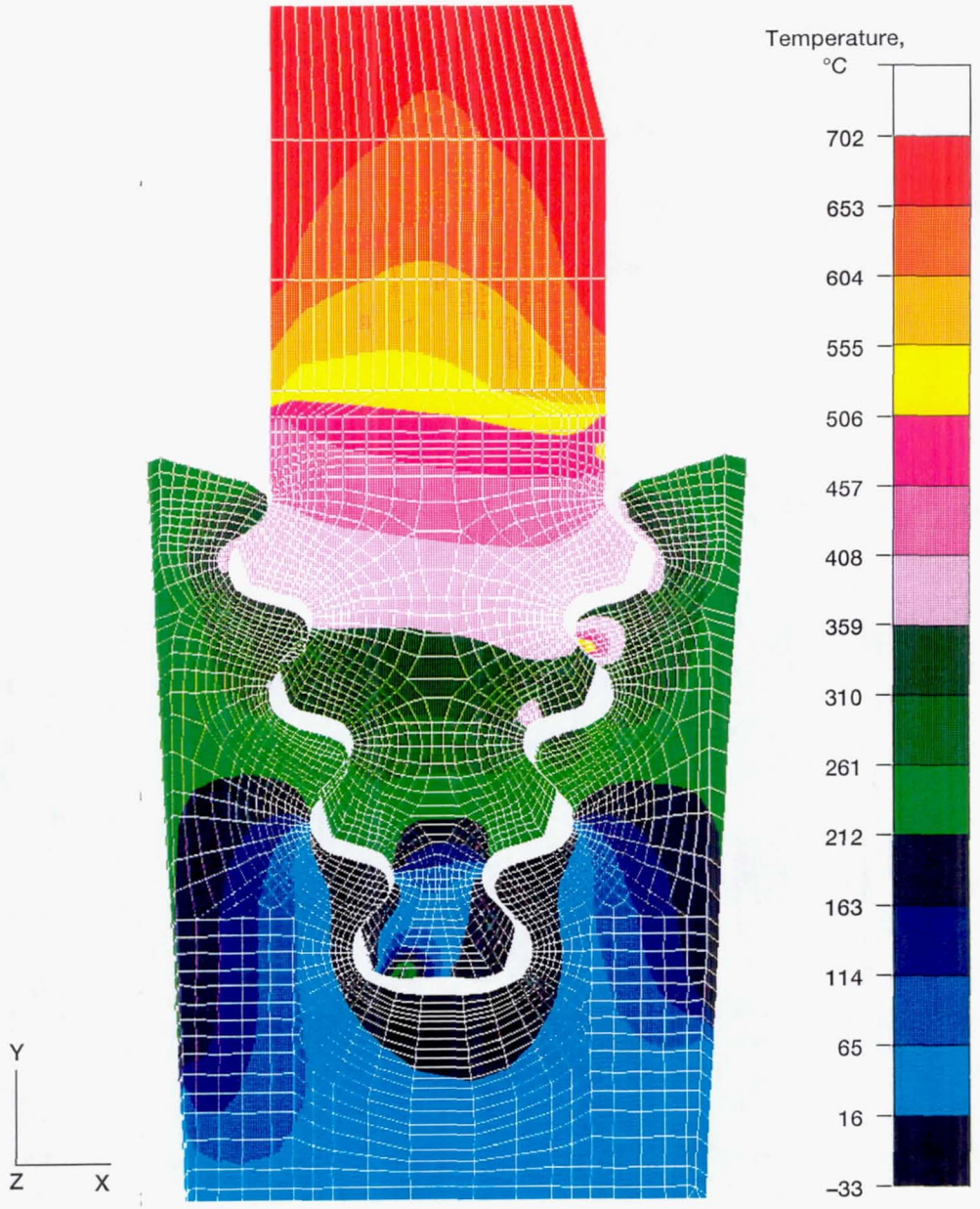

Figure 7.—Temperature at second ignition spike condition.

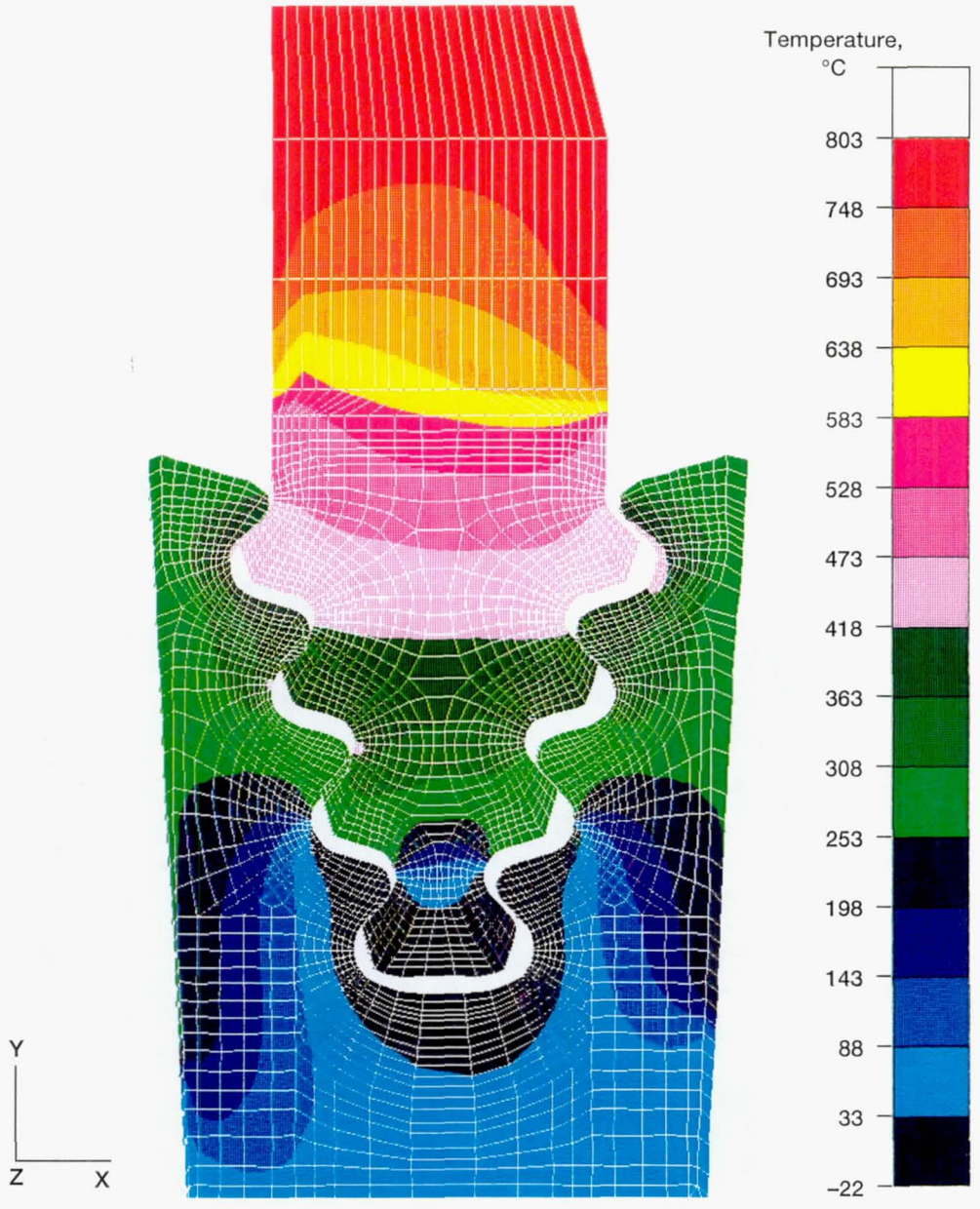

Figure 8.—Temperature at cruise condition of blade.

Figure 9.—Temperature at engine shutdown condition.

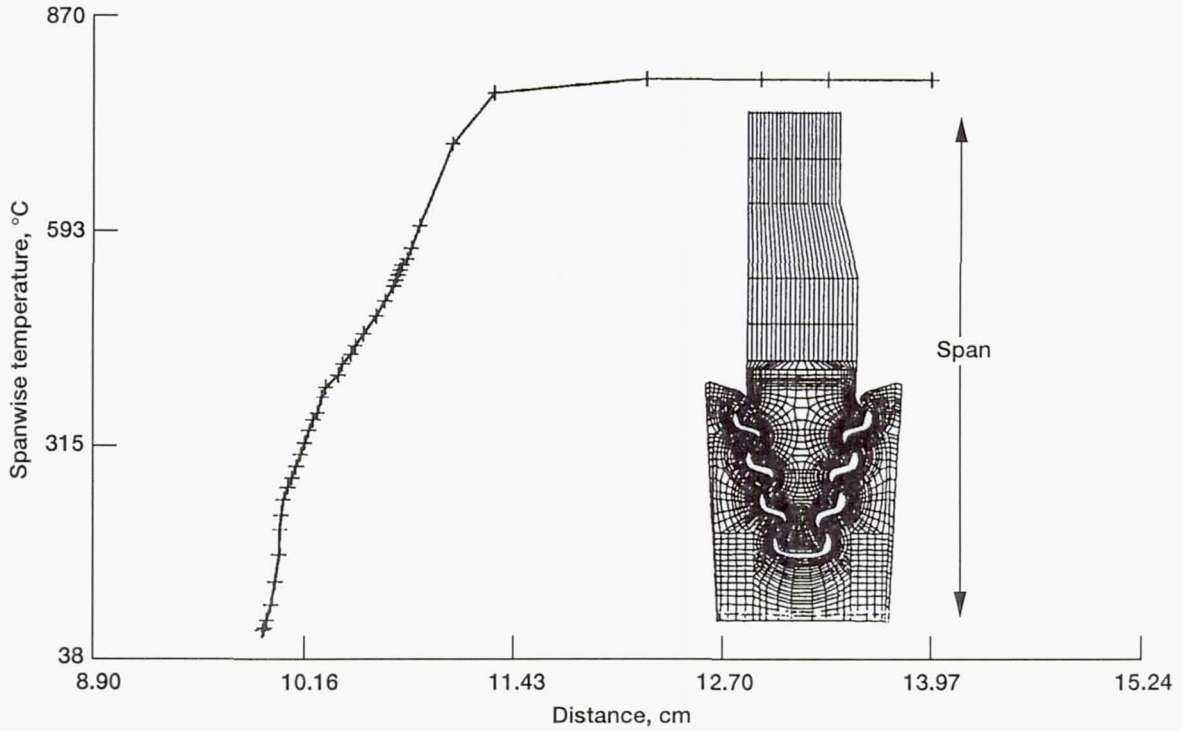

Figure 10.—Temperature gradient along span direction.

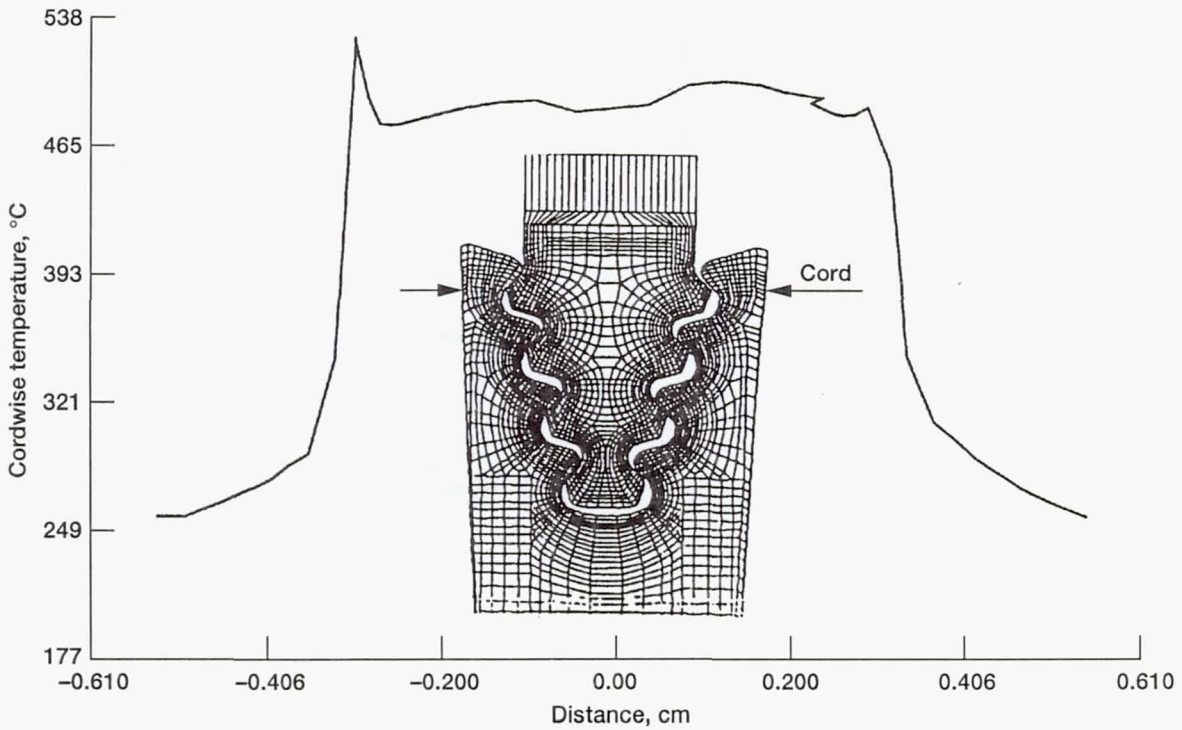

Figure 11.—Temperature gradient along cord direction.

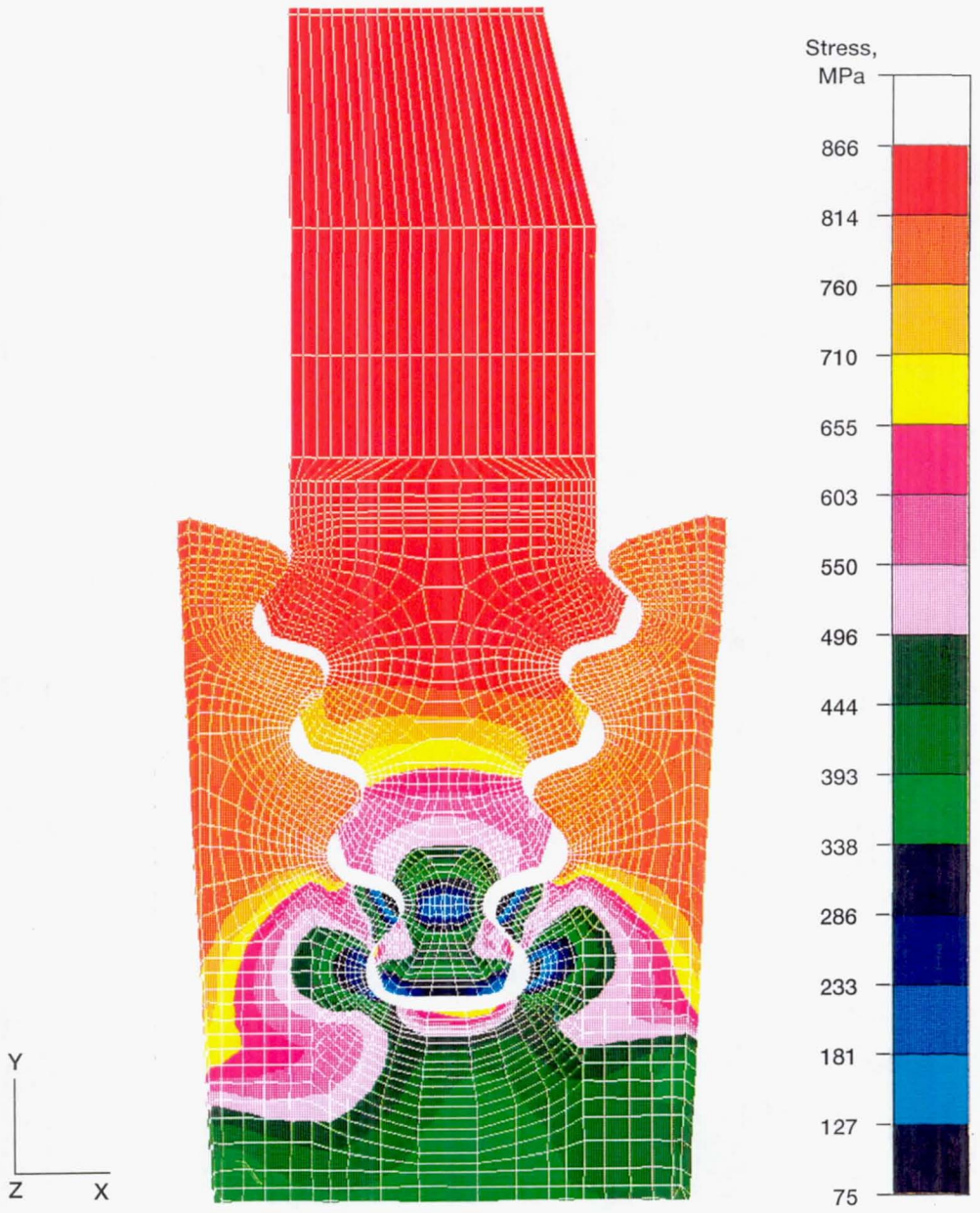

Figure 12.—Distribution of Von-Mises-equivalent stresses during first ignition spike.

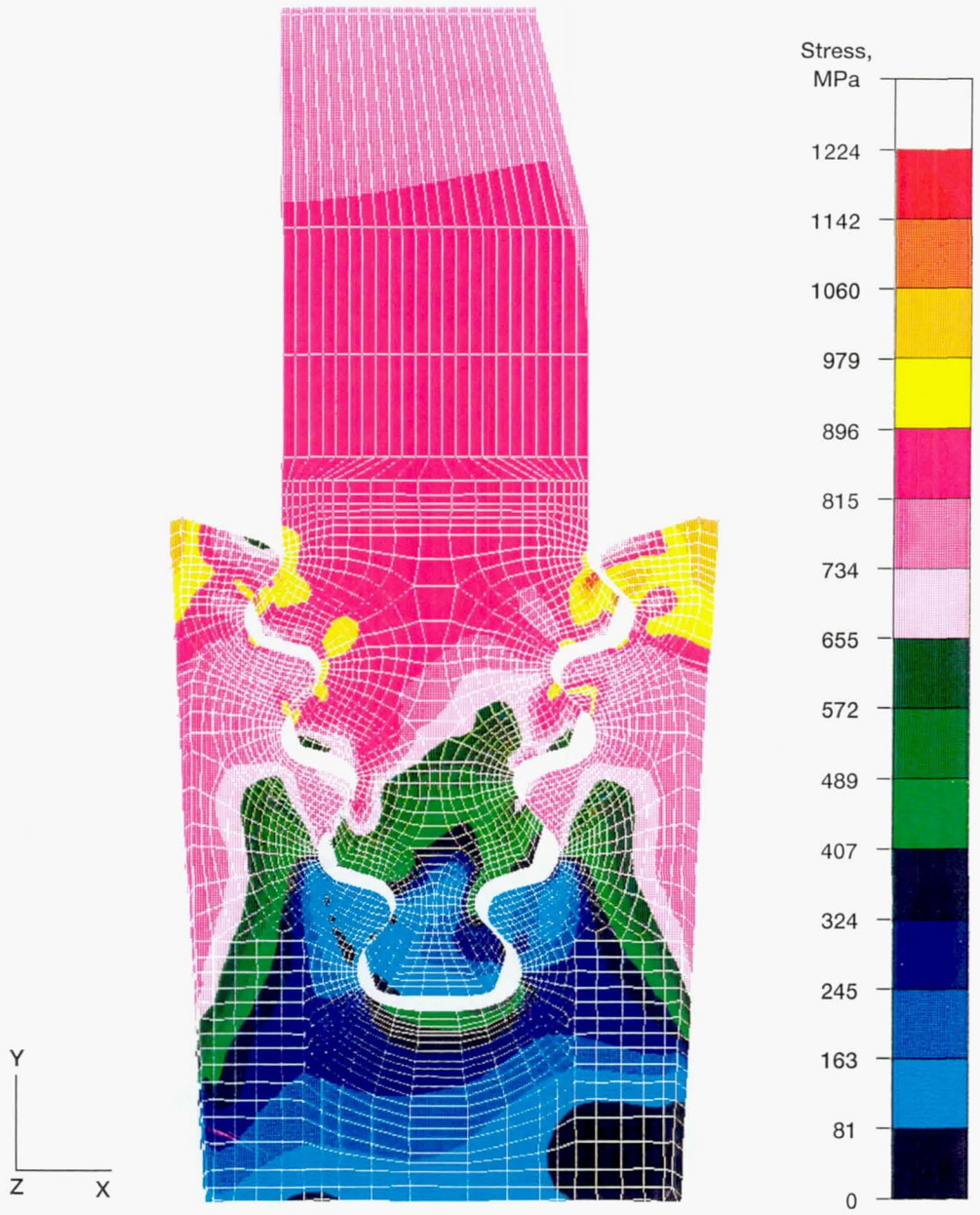

Figure 13.—Distribution of Von-Mises-equivalent stresses under cruise conditions.

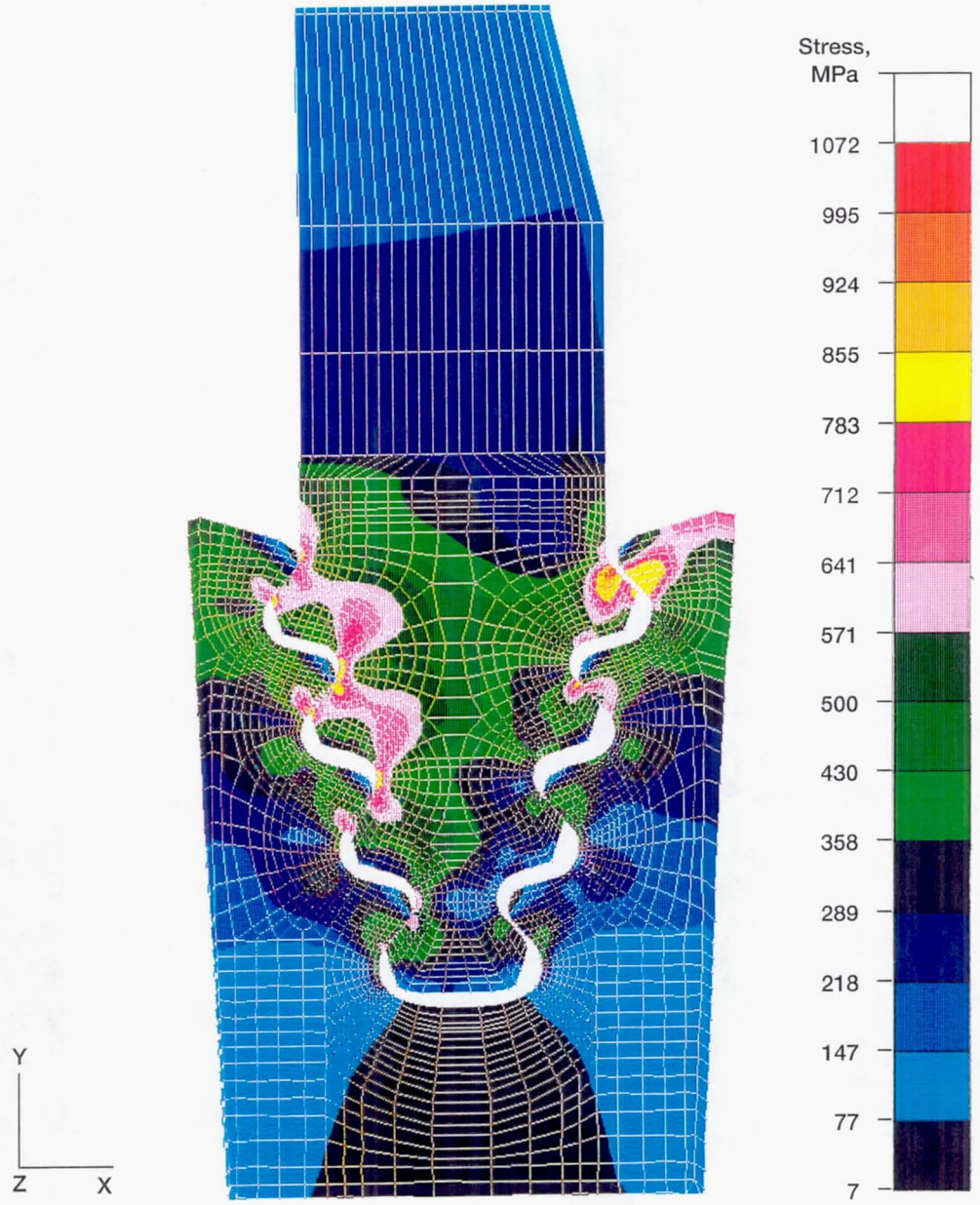

Figure 14.—Von-Mises-equivalent stresses under centrifugal loading.

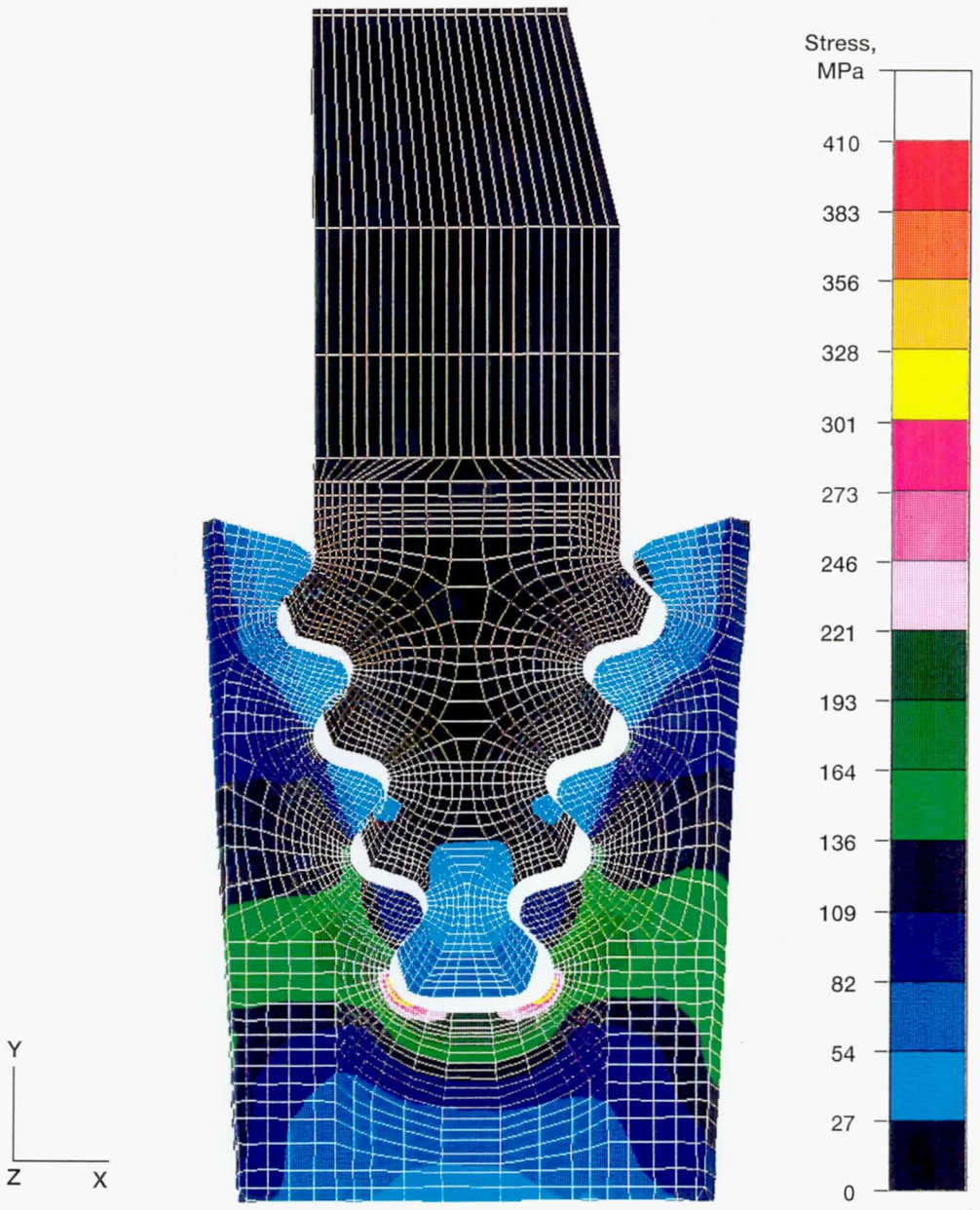

Figure 15.—Von-Mises-equivalent stresses during shutdown conditions.

REPORT DOCUMENTATION PAGE

Form Approved
OMB No. 0704-0188

1. AGENCY USE ONLY (*Leave blank*)	2. REPORT DATE	3. REPORT TYPE AND DATES COVERED
	June 1996	Final Contractor Report

4. TITLE AND SUBTITLE

Structural Evaluation of a Space Shuttle Main Engine (SSME) High Pressure Fuel Turbopump Turbine Blade

5. FUNDING NUMBERS

WU–505–63–5B
C–NAS3–27186

6. AUTHOR(S)

Ali Abdul-Aziz

7. PERFORMING ORGANIZATION NAME(S) AND ADDRESS(ES)

NYMA, Inc.
2001 Aerospace Parkway
Brook Park, Ohio 44142

8. PERFORMING ORGANIZATION REPORT NUMBER

E–10018

9. SPONSORING/MONITORING AGENCY NAME(S) AND ADDRESS(ES)

National Aeronautics and Space Administration
Lewis Research Center
Cleveland, Ohio 44135–3191

10. SPONSORING/MONITORING AGENCY REPORT NUMBER

NASA CR–198428

11. SUPPLEMENTARY NOTES

Project Manager, Rod Ellis, Structures Division, NASA Lewis Research Center, organization code 5220, (216) 433–3340.

12a. DISTRIBUTION/AVAILABILITY STATEMENT

Unclassified - Unlimited
Subject Category 39

This publication is available from the NASA Center for Aerospace Information, (301) 621–0390.

12b. DISTRIBUTION CODE

13. ABSTRACT ***(Maximum 200 words)***

Thermal and structural finite-element analyses were performed on the first high pressure fuel turbopump turbine blade of the space shuttle main engine (SSME). A two-dimensional (2-D) finite-element model of the blade and firtree disk attachment was analyzed using the general purpose MARC (finite-element) code. The loading history applied is a typical test stand engine cycle mission, which consists of a startup condition with two thermal spikes, a steady state and a shutdown transient. The blade material is a directionally solidified (DS) Mar-M 246 alloy, the blade rotor is forged with waspalloy material. Thermal responses under steady-state and transient conditions were calculated. The stresses and strains under the influence of mechanical and thermal loadings were also determined. The critical regions that exhibited high stresses and severe localized plastic deformation were the blade-rotor gaps.

14. SUBJECT TERMS

Finite element; Thermal and structural; Transient analysis; Stress-strain histories

15. NUMBER OF PAGES
20

16. PRICE CODE
A03

17. SECURITY CLASSIFICATION OF REPORT	18. SECURITY CLASSIFICATION OF THIS PAGE	19. SECURITY CLASSIFICATION OF ABSTRACT	20. LIMITATION OF ABSTRACT
Unclassified	Unclassified	Unclassified	